Electronic Supplementary Material (ESI) for Nanoscale.
This journal is © The Royal Society of Chemistry 2022

Looking at platinum carbonyl nanoclusters as *superatoms*

Jianyu Wei,[a,b] Rémi Marchal,[a] Didier Astruc,[b] Samia Kahlal*[a] Jean-François Halet,*[a,c] and Jean-Yves Saillard*[a]

[a] Univ Rennes, CNRS, Institut des Sciences Chimiques de Rennes (ISCR) – UMR 6226, F 35000 Rennes, France. E-mail: samia.kahlal@univ-rennes1.fr, saillard@univ-rennes1.fr

[b] ISM, UMR CNRS 5255, University of Bordeaux, 351 Cours de la Libération, F-33405 Talence Cedex, France.

[c] CNRS – Saint-Gobain – NIMS, IRL 3629, Laboratory for Innovative Key Materials and Structures (LINK), National Institute for Materials Science (NIMS), Tsukuba, 305-0044, Japan. E-mail: jean-francois.halet@univ-rennes1.fr

Dedicated to the memory of Professor Larry F. Dahl, a pioneer and an immense contributor to ligated cluster chemistry

Table of Contents

Fig. S1 Metallic kernel structure of the icosahedral 8-electron *superatom* models. Light-grey, pink and golden-yellow spheres are outer Pt, central Pt and Au atoms, respectively. 5

Fig. S2 Plots of the *superatomic* orbitals of $[Pt_{13}(CO)_{12}]^{8-}$ (I_h) with the surface isovalue of ± 0.02 $(e/bohr^3)^{1/2}$. 6

Fig. S3 Kohn-Sham orbital diagram of $Pt_{13}Au_4(\mu_2\text{-}CO)_2(CO)_{16}$. The 5d block contains all Pt and Au contributions. 7

Fig. S4 Kohn-Sham orbital diagram of $Pt_{17}(\mu_2\text{-}CO)_4(CO)_{16}$. The 5d block contains all Pt contributions. 8

Fig. S5 Metallic kernel structure of $[Pt_{13}(CO)_{12}(\mu\text{-}CO)_5]^{2-}$, $[Pt_{14}(CO)_{12}(\mu\text{-}CO)_6]^{4-}$ and $[Pt_{15}(CO)_{11}(\mu\text{-}CO)_8]^{4-}$. Light-grey and pink spheres are outer Pt and central Pt, respectively…9

Fig. S6 Plots of the *superatomic* orbitals of $[Pt_{13}(CO)_{12}(\mu\text{-}CO)_5]^{2-}$ (D_{5h}) with the surface isovalue of ± 0.02 $(e/bohr^3)^{1/2}$. 10

Fig. S7 The occupied 6s(Pt) combinations of $[Pt_{14}(\mu\text{-}CO)_6(CO)_{12}]^{4-}$ and $[Pt_{15}(\mu\text{-}CO)_8(CO)_{11}]^{4-}$. 11

Fig. S8 Metallic kernel structure of the clusters that can be viewed as assemblies of individual superatoms. Light-grey, pink and green spheres are outer Pt, central Pt and the Pt that shared between two or three *superatoms*, respectively. 12

Fig. S9 Plots of the *supermolecular* orbitals of $[Pt_{19}(CO)_{17}]^{10-}$ (D_{5h}) with the surface isovalue of ± 0.02 $(e/bohr^3)^{1/2}$. 13

Fig. S10 Spin density plots of $[Pt_{19}(CO)_{17}\{Cd_5(\mu\text{-}Br)_5Br_3(Me_2CO)_2\}\{Cd_5(\mu\text{-}Br)_5Br(Me_2CO)_4\}]^{2-}$ (A) and $[Pt_{19}CO_{17}]^{8-}$ (D_{5h}) (B). 14

Fig. S11 Kohn-Sham orbital diagram of the fully decorated $[Pt_{19}(CO)_{17}\{Cd_5(\mu\text{-}Br)_5Br_3(Me_2CO)_2\}\{Cd_5(\mu\text{-}Br)_5Br(Me_2CO)_4\}]^{4-}$. 15

Fig. S12 Kohn-Sham orbital diagram of $[Pt_{26}(\mu_2\text{-}CO)_9(CO)_{23}]^{2-}$. The *supermolecular* orbitals plotted on the right side are reminiscent of the valence orbitals of the hypothetical triangular isomer of O_3. 16

Fig. S13 Metallic kernel structure of the linear assemblies of individual icosahedral superatoms (hypothetical models). Light-grey, pink and green spheres are outer Pt, central Pt and the Pt that shared between two or three *superatoms*, respectively.....17

Fig. S14 Kohn-Sham orbital diagram of the hypothetical $Pt_{25}(CO)_{22}]^{12-}$.....18

Fig. S15 Kohn-Sham orbital diagram of the hypothetical $[Pt_{23}(CO)_{20}]^{12-}$ 19

Fig. S16 Kohn-Sham orbital diagram of the hypothetical $[Pt_{23}(CO)_{21}]^{10-}$ 20

Fig. S17 Metallic kernel structure of various clusters with non-spherical 3D structure. Light-grey, pink and golden-yellow spheres are outer Pt, inner Pt that belonging to the encapsulated polyhedron and Au atoms, respectively.....21

Fig. S18 Kohn-Sham orbital diagram of the pseudo-spherical $[Pt_{38}(\mu_2\text{-}CO)_{12}(CO)_{32}]^{2-}$.....22

Fig. S19 Kohn-Sham MO diagram of $[Pt_{36}(\mu\text{-}CO)_{18}(CO)_{26}]^{2-}$. The *supermolecular* orbitals, plotted on the right side, are consistent with the $1S^2\ 1P^8\ 1D^{10}$ configuration. 23

Fig. S20 Qualitative frontier MO interaction diagram between the Ptn(CO)n and (μ-CO)m fragments in a neutral [Ptn(CO)n(μ-CO)m] nanocluster.....24

Table S1. Relevant computed data for $[Pt_{13}(CO)_{12}]^{8-}$.....25

Table S2. Relevant computed data for $[Pt_{13}(CO)_{12}\{Cd_5(\mu\text{-}Br)_5Br_2(dmf)_3\}_2]^{2-}$ 26

Table S3. Relevant computed data for the $Pt_{13}(Au_2L_2)_2(\mu\text{-}CO)_2(CO)_8(L)_4$ (L = CO, PH_3) clusters. 27

Table S4. Relevant computed data for the $Pt_{13}(Pt_2(\mu\text{-}CO)(L)_2)_2(\mu\text{-}CO)_2(CO)_8(L)_4$ (L = CO, PH_3) clusters. 28

Table S5. Relevant computed data for the $[Pt_{14}(\mu\text{-}CO)_6(CO)_{12}]^{4-}$ and $[Pt_{15}(\mu\text{-}CO)_8(CO)_{11}]^{4-}$ clusters. 28

Table S6. Relevant computed data for the $[Pt_{19}(CO)_{17}]^{8-/10-}$ clusters.....29

Table S7. Computed data for $[Pt_{19}(CO)_{17}\{Cd_5(\mu\text{-}Br)_5Br_3(Me_2CO)_2\}\{Cd_5(\mu\text{-}Br)_5Br(Me_2CO)_4\}]^{x-}$ (x = 2, 4).....30

Table S8. Relevant computed data for $[Pt_{19}(\mu\text{-}CO)_{10}(CO)_{12}]^{4-}$. 31

Table S9. Relevant computed data for $[Pt_{26}(\mu\text{-}CO)_9(CO)_{23}]^{2-}$. 32

Table S10. Relevant computed data for $[Pt_{23}(\mu\text{-}CO)_{13}(CO)_{14}]^{2-}$. 33

Table S11. Relevant computed data for the hypothetical cluster $[Pt_{25}(CO)_{22}]^{12-}$. 33

Table S12. Relevant computed data for the hypothetical cluster $[Pt_{23}CO_{20}]^{12-}$.....34

Table S13. Relevant computed data for the hypothetical cluster $[Pt_{23}CO_{21}]^{10-}$. 34

Table S14. Relevant computed data for $[Pt_{38}(\mu\text{-}CO)_{12}(CO)_{32}]^{2-}$. 34

Table S15. Relevant computed data for $[Pt_{36}(\mu\text{-}CO)_{18}(CO)_{26}]^{2-}$. 35

Table S16. Relevant computed data for $[Pt_{19}(\mu_3\text{-}CO)_3(\mu\text{-}CO)_3(CO)_{18}(\mu_4\text{-}AuPH_3)_3]^{-}$. 36

Table S17. Relevant computed data for $[Pt_{19}(\mu_3\text{-}CO)(\mu\text{-}CO)_5(CO)_{18}\{\mu_4\text{-}Au_2(PH_3)_2\}_2]$.....36

Table S18. Relevant computed data for $[Pt_{40}(\mu\text{-}CO)_{16}(CO)_{24}]^{6-}$. 37

Table S19. Relevant computed data for $[Pt_{24}(\mu\text{-}CO)_8(CO)_{22}]^{2-}$.....37

Table S20. Relevant computed data for $[Pt_{33}(\mu\text{-}CO)_{10}(CO)_{28}]^{2-}$. 38

References.....38

Computed model	Metallic kernel structure
$[Pt_{13}(CO)_{12}]^{8-}$	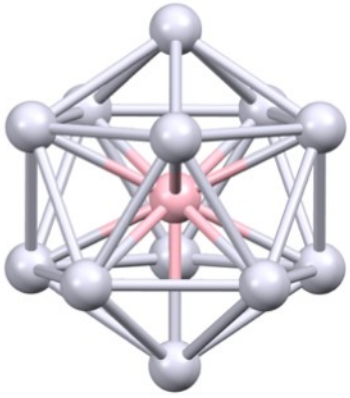
$[Pt_{13}Au_4(\mu\text{-}CO)_2(CO)_{16}]$	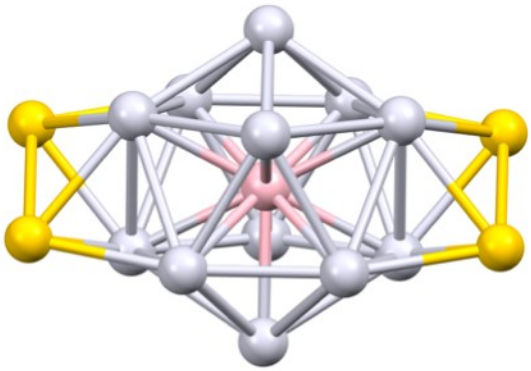
$[Pt_{17}(\mu\text{-}CO)_4(CO)_{16}]$	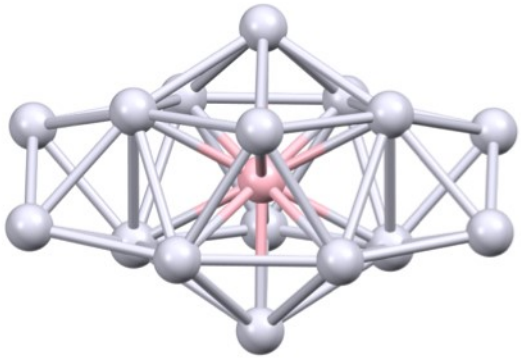

Fig. S1 Metallic kernel structure of the icosahedral 8-electron *superatom* models. Light-grey, pink and golden-yellow spheres are outer Pt, central Pt and Au atoms, respectively.

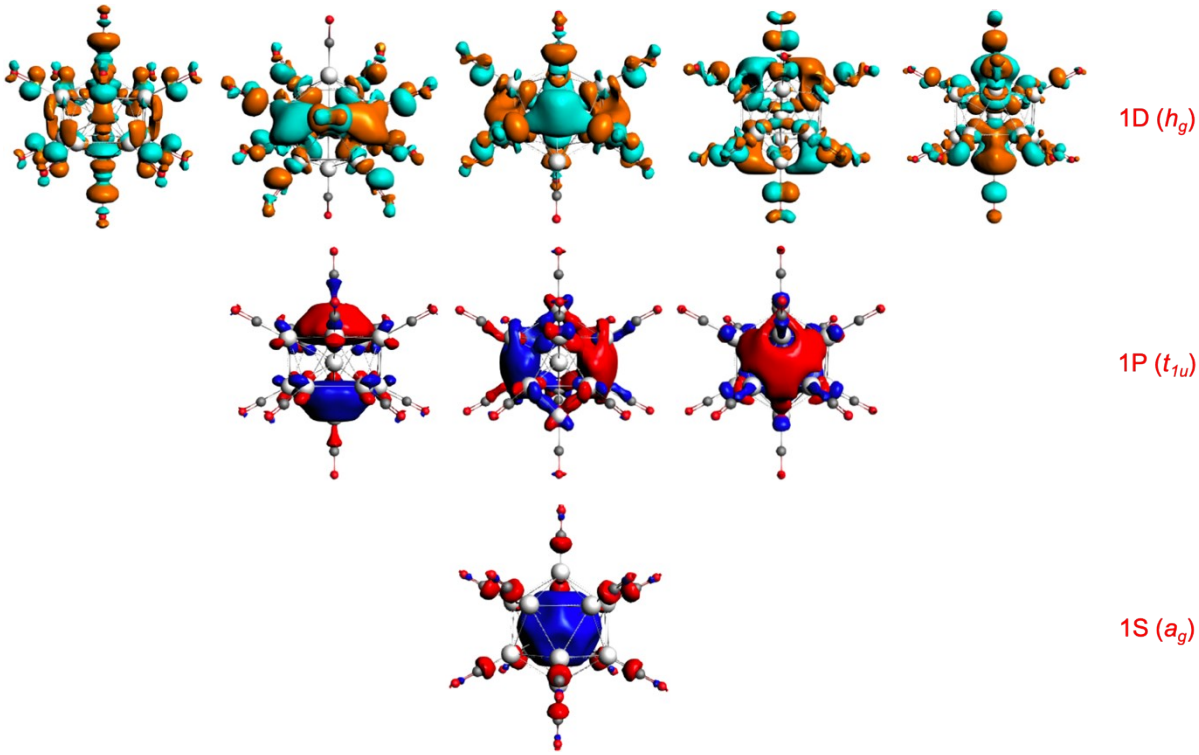

Fig. S2 Plots of the *superatomic* orbitals of $[Pt_{13}(CO)_{12}]^{8-}$ (I_h) with the surface isovalue of ± 0.02 $(e/bohr^3)^{1/2}$.

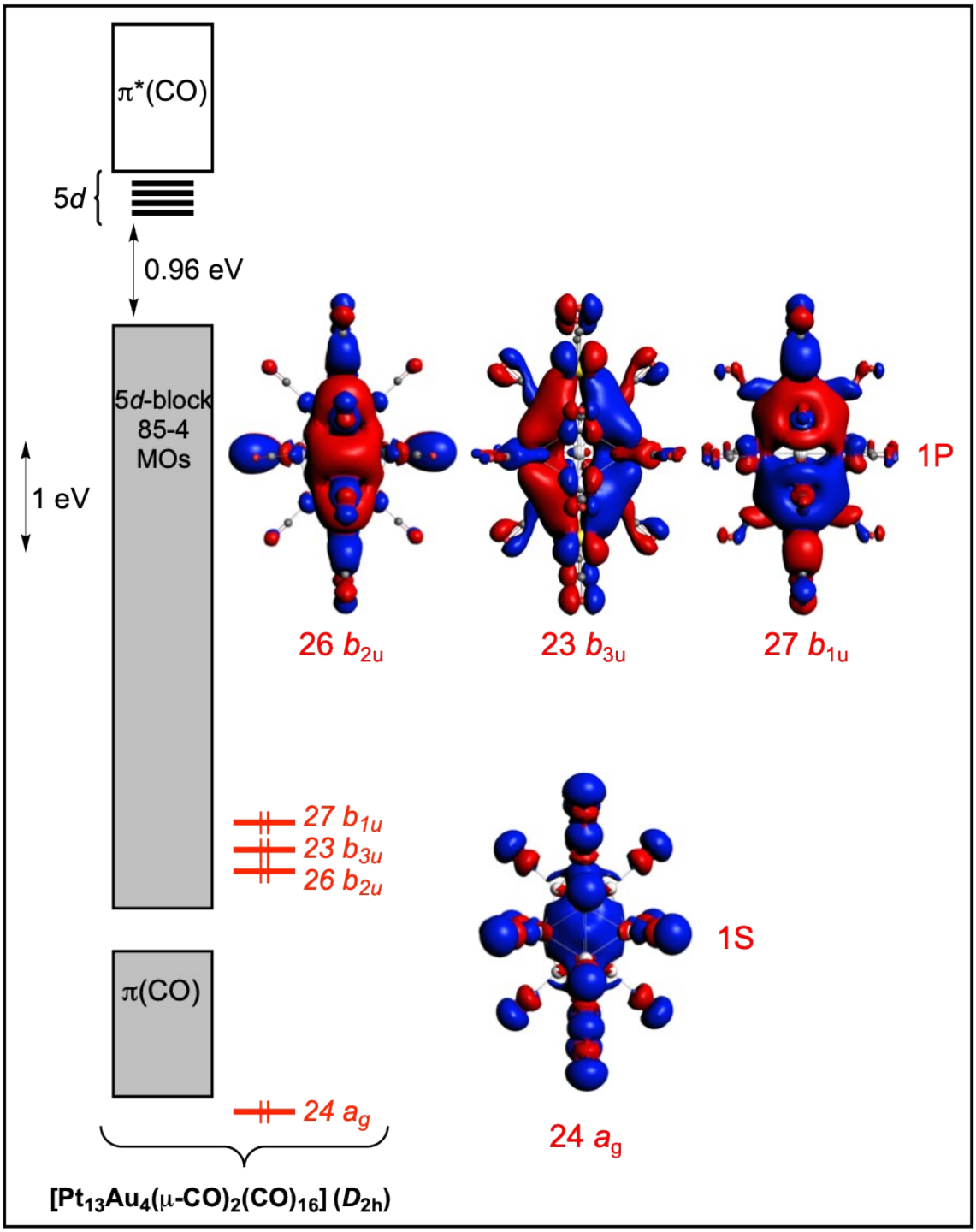

Fig. S3 Kohn-Sham orbital diagram of $Pt_{13}Au_4(\mu_2\text{-}CO)_2(CO)_{16}$. The 5d block contains all Pt and Au contributions. The surface isovalue of the inserted plots of *superatomic* orbitals is ± 0.01 $(e/bohr^3)^{1/2}$.

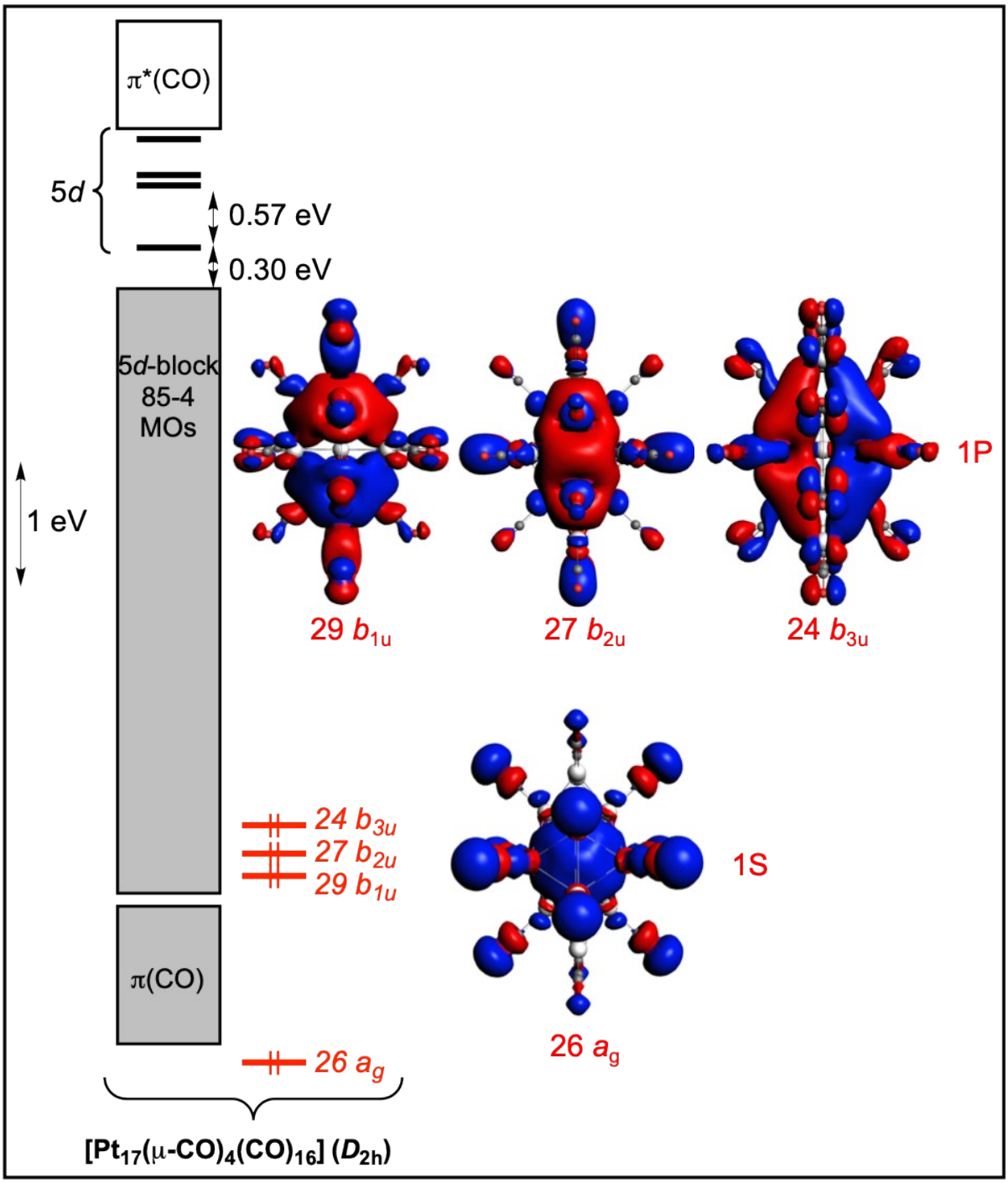

Fig. S4 Kohn-Sham orbital diagram of $Pt_{17}(\mu_2\text{-}CO)_4(CO)_{16}$. The 5d block contains all Pt contributions. The surface isovalue of the inserted plots of *superatomic* orbitals is ± 0.01 $(e/bohr^3)^{1/2}$.

Computed model	Metallic kernel structure
$[Pt_{13}(\mu\text{-}CO)_5(CO)_{12}]^{2-}$	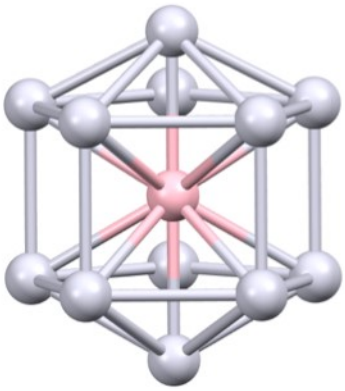
$[Pt_{14}(\mu\text{-}CO)_6(CO)_{12}]^{4-}$	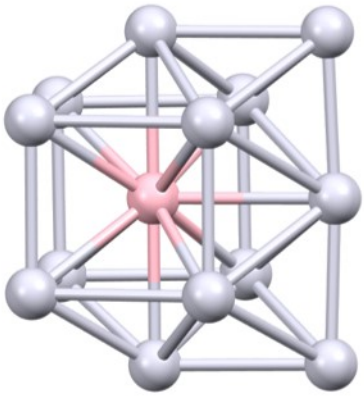
$[Pt_{15}(\mu\text{-}CO)_8(CO)_{11}]^{4-}$	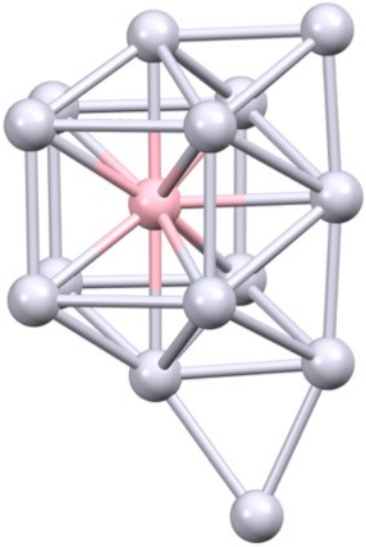

Fig. S5 Metallic kernel structure of $[Pt_{13}(CO)_{12}(\mu\text{-}CO)_5]^{2-}$, $[Pt_{14}(CO)_{12}(\mu\text{-}CO)_6]^{4-}$ and $[Pt_{15}(CO)_{11}(\mu\text{-}CO)_8]^{4-}$. Light-grey and pink spheres are outer Pt and central Pt, respectively.

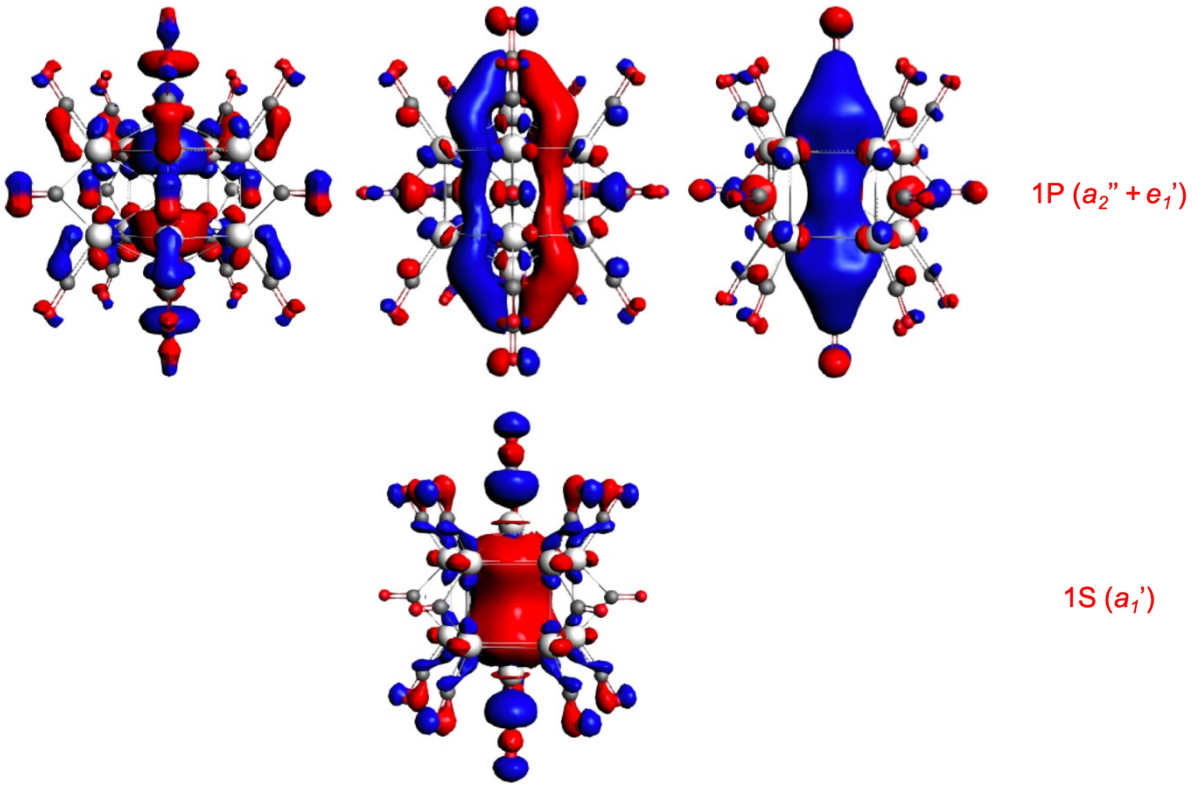

Fig. S6 Plots of the *superatomic* orbitals of $[Pt_{13}(CO)_{12}(\mu\text{-}CO)_5]^{2-}$ (D_{5h}) with the surface isovalue of ± 0.02 $(e/bohr^3)^{1/2}$.

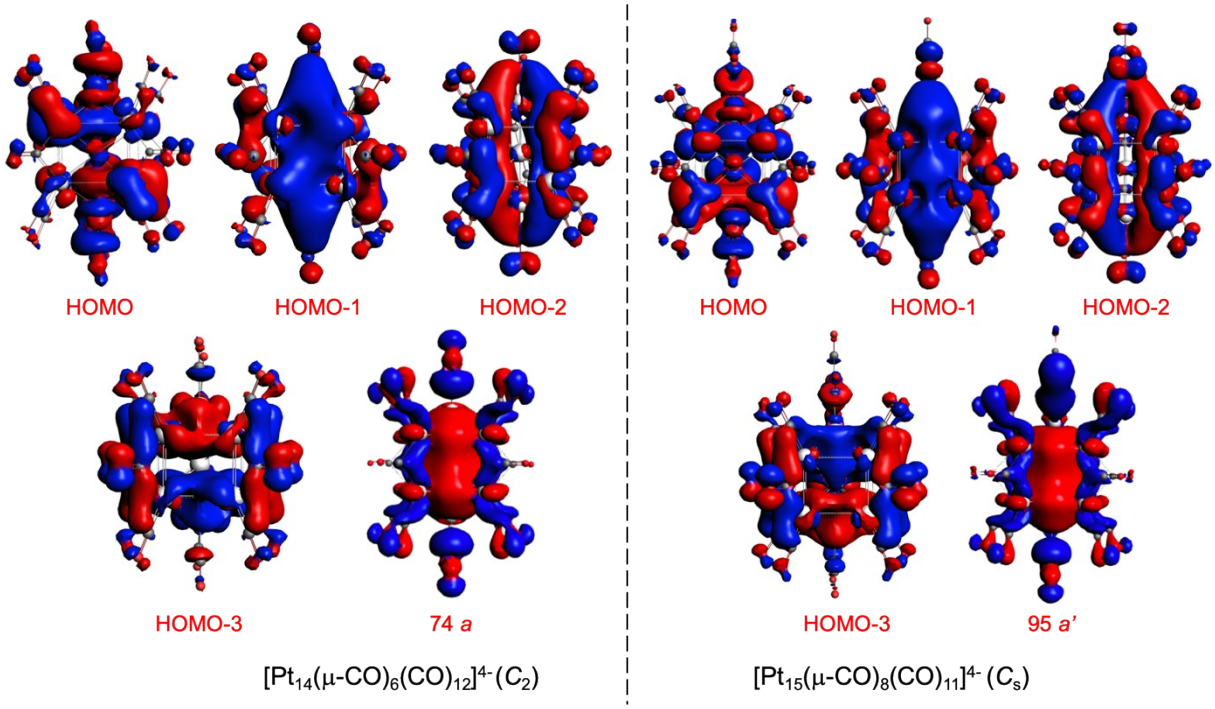

Fig. S7 The occupied 6s(Pt) combinations of $[Pt_{14}(\mu\text{-}CO)_6(CO)_{12}]^{4-}$ and $[Pt_{15}(\mu\text{-}CO)_8(CO)_{11}]^{4-}$. The surface isovalue of the inserted plots of orbitals is ± 0.01 $(e/bohr^3)^{1/2}$.

Computed model	Metallic kernel structure
$[Pt_{19}(CO)_{17}]^{8-/10-}$	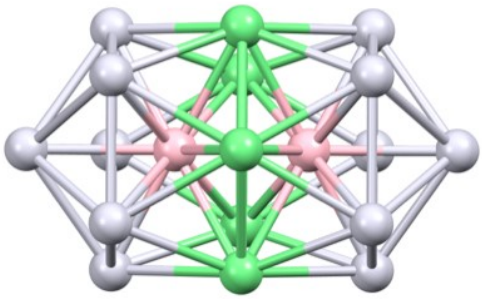
$[Pt_{19}(\mu\text{-}CO)_{10}(CO)_{12}]^{4-}$	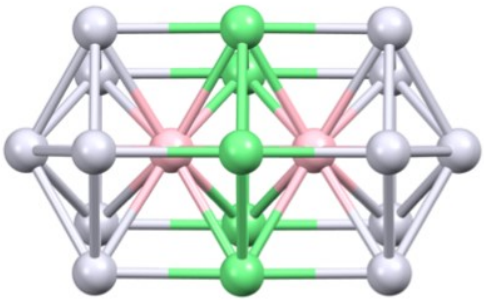
$[Pt_{26}(\mu\text{-}CO)_{9}(CO)_{23}]^{2-}$	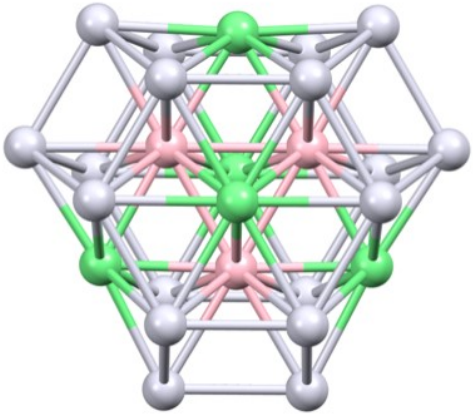
$[Pt_{23}(\mu\text{-}CO)_{13}(CO)_{14}]^{2-}$	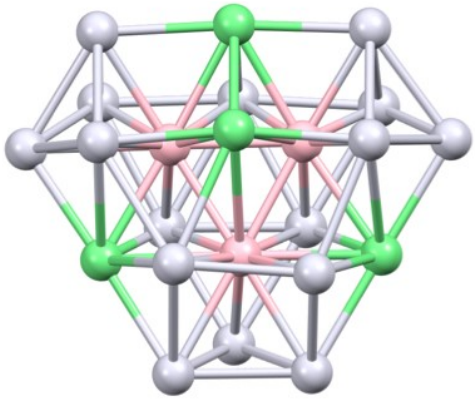

Fig. S8 Metallic kernel structure of the clusters that can be viewed as assemblies of individual superatoms. Light-grey, pink and green spheres are outer Pt, central Pt and the Pt shared between two or three *superatoms*, respectively.

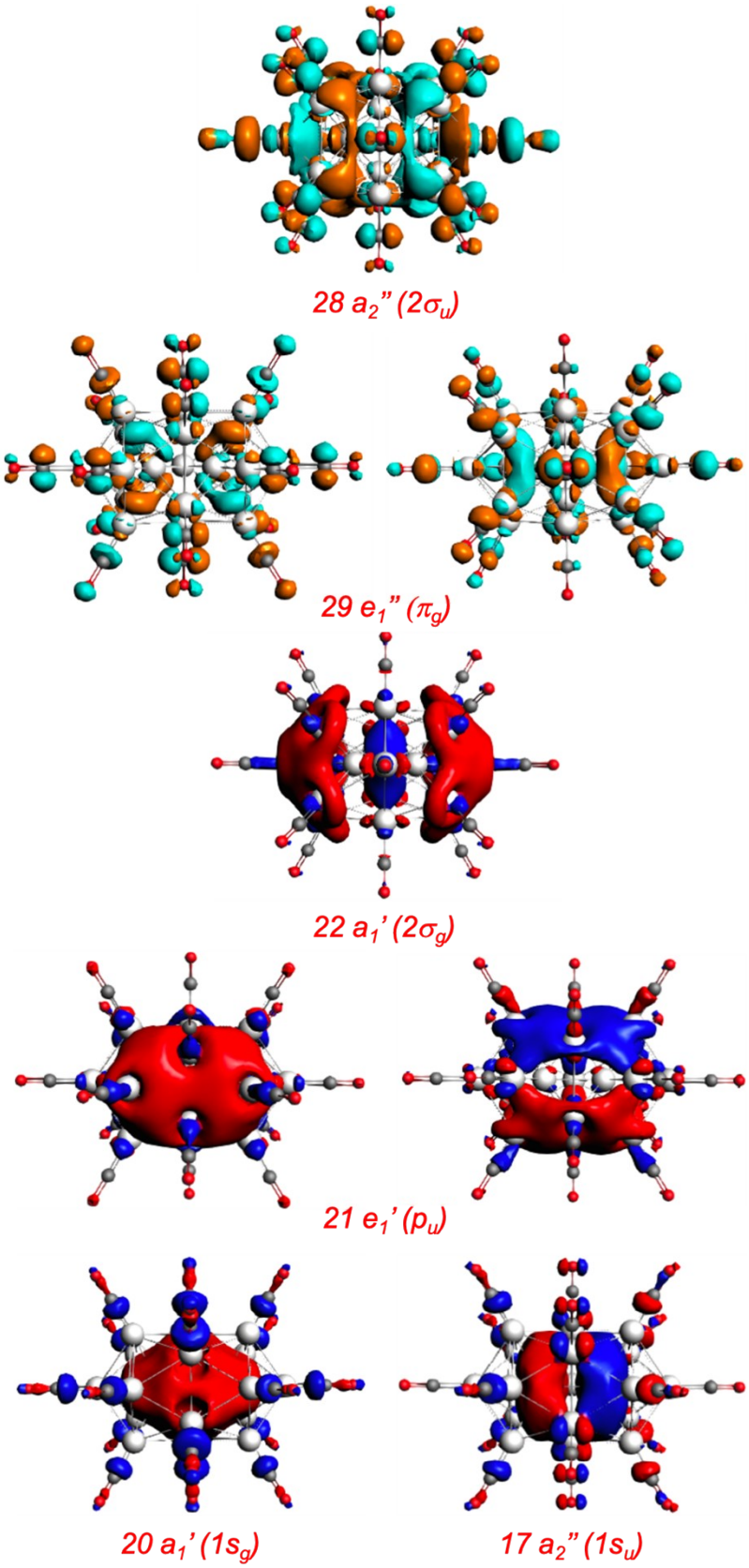

Fig. S9 Plots of the *supermolecular* orbitals of $[Pt_{19}(CO)_{17}]^{10-}$ (D_{5h}) with the surface isovalue of ± 0.02 $(e/bohr^3)^{1/2}$.

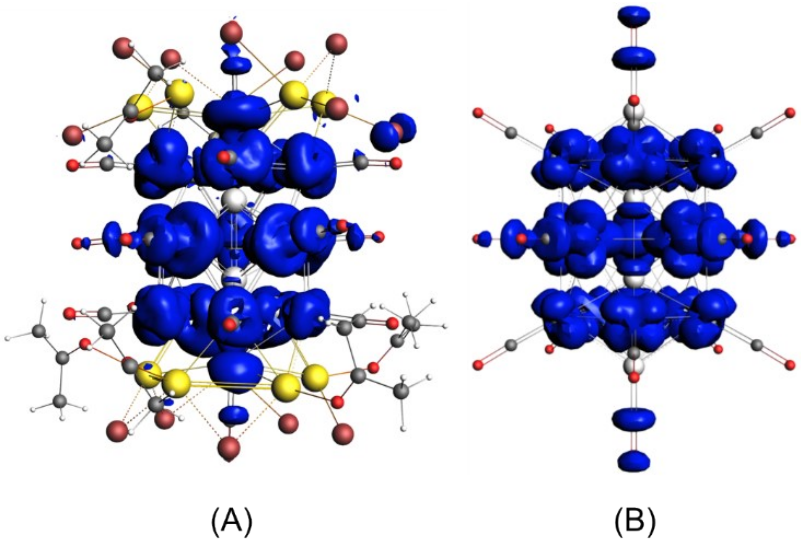

Fig. S10 Spin density plots of $[Pt_{19}(CO)_{17}\{Cd_5(\mu\text{-}Br)_5Br_3(Me_2CO)_2\}\{Cd_5(\mu\text{-}Br)_5Br(Me_2CO)_4\}]^{2-}$ (A) and $[Pt_{19}CO_{17}]^{8-}$ (D_{5h}) (B).

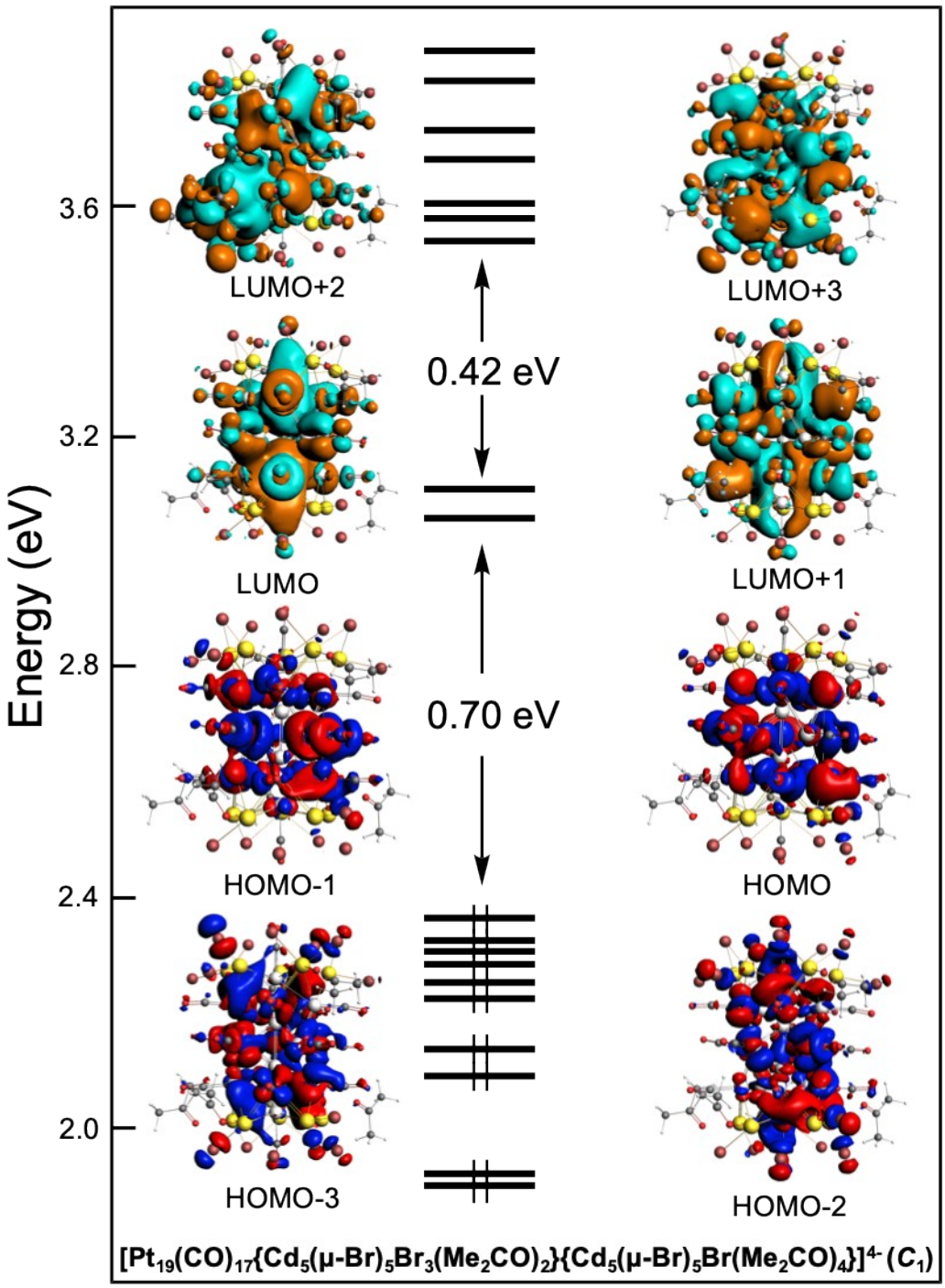

Fig. S11 Kohn-Sham frontier molecular orbital diagram of the fully decorated $[Pt_{19}(CO)_{17}\{Cd_5(\mu\text{-}Br)_5Br_3(Me_2CO)_2\}\{Cd_5(\mu\text{-}Br)_5Br(Me_2CO)_4\}]^{4-}$. The surface isovalue of the inserted plots of orbitals is ± 0.02 $(e/bohr^3)^{1/2}$.

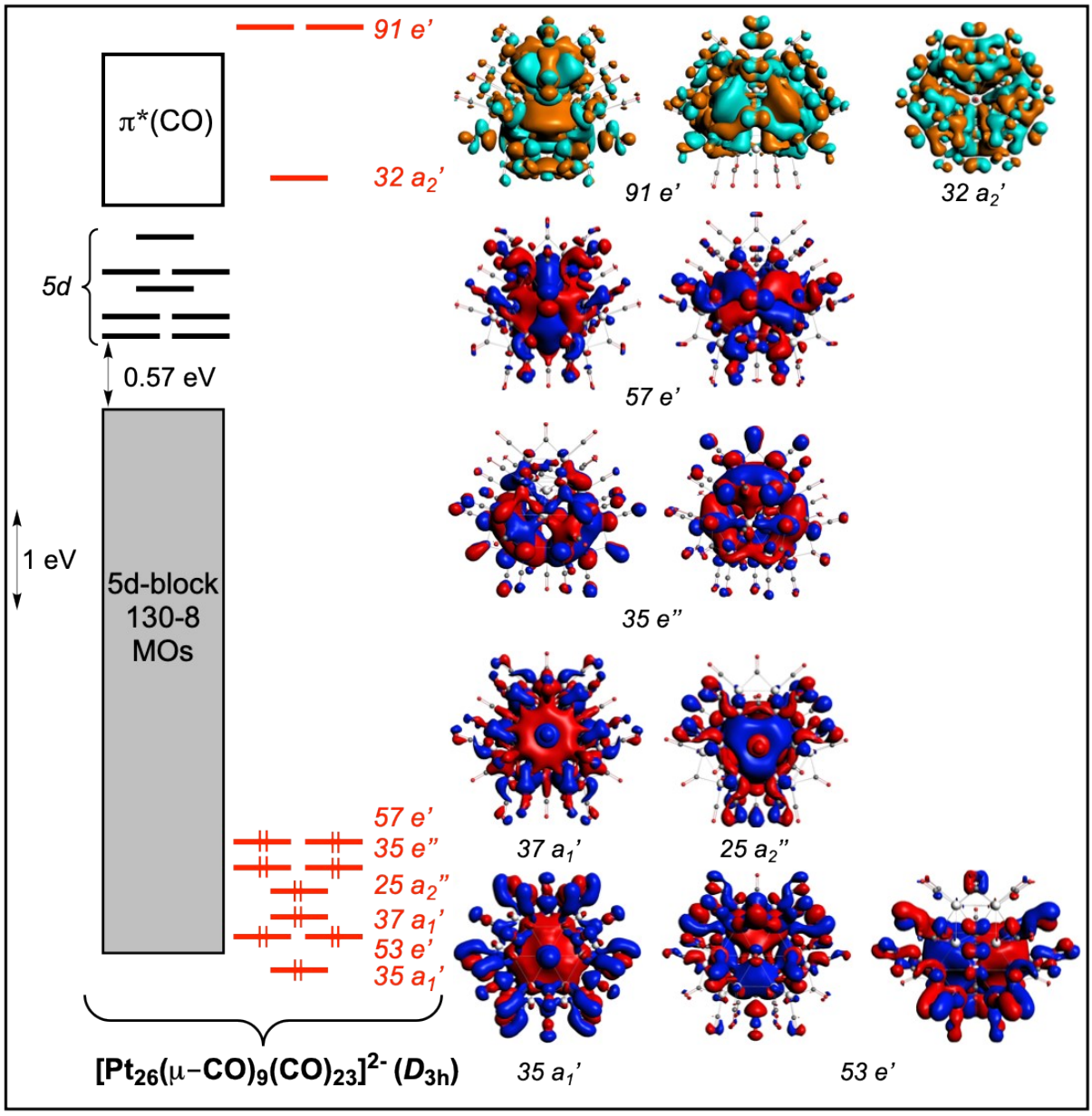

Fig. S12 Kohn-Sham orbital diagram of $[Pt_{26}(\mu_2\text{-}CO)_9(CO)_{23}]^{2-}$. The *supermolecular* orbitals plotted on the right side are reminiscent of the valence orbitals of the hypothetical triangular isomer of O_3. The surface isovalue of the inserted plots of *supermolecular* orbitals is ± 0.01 $(e/bohr^3)^{1/2}$.

Computed model	Metallic kernel structure
$[Pt_{25}(CO)_{22}]^{12-}$ (D_{5d})	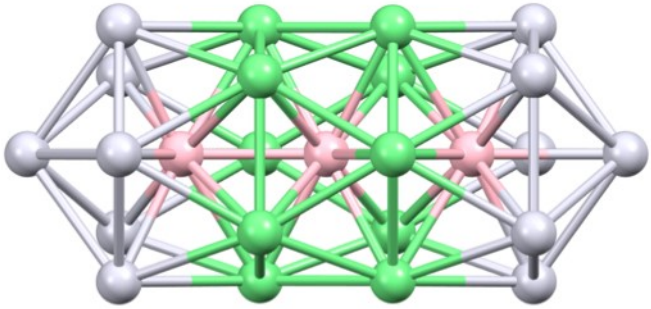
$[Pt_{23}(CO)_{20}]^{12-}$ (D_{3h})	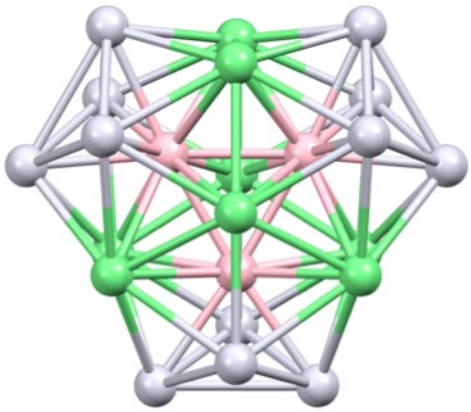
$[Pt_{23}(CO)_{21}]^{10-}$ (D_{3h})	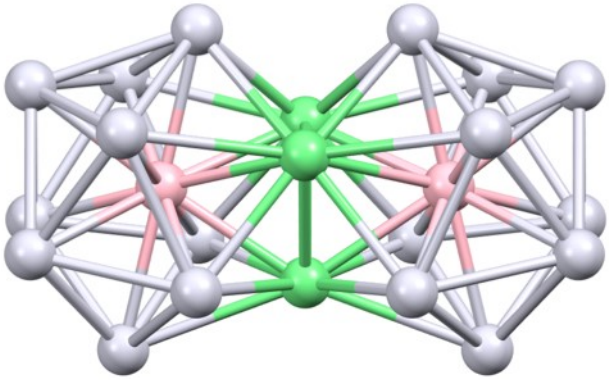

Fig. S13 Metallic kernel structure of the linear assemblies of individual icosahedral superatoms (hypothetical models). Light-grey, pink and green spheres are outer Pt, central Pt and the Pt shared between two or three *superatoms*, respectively.

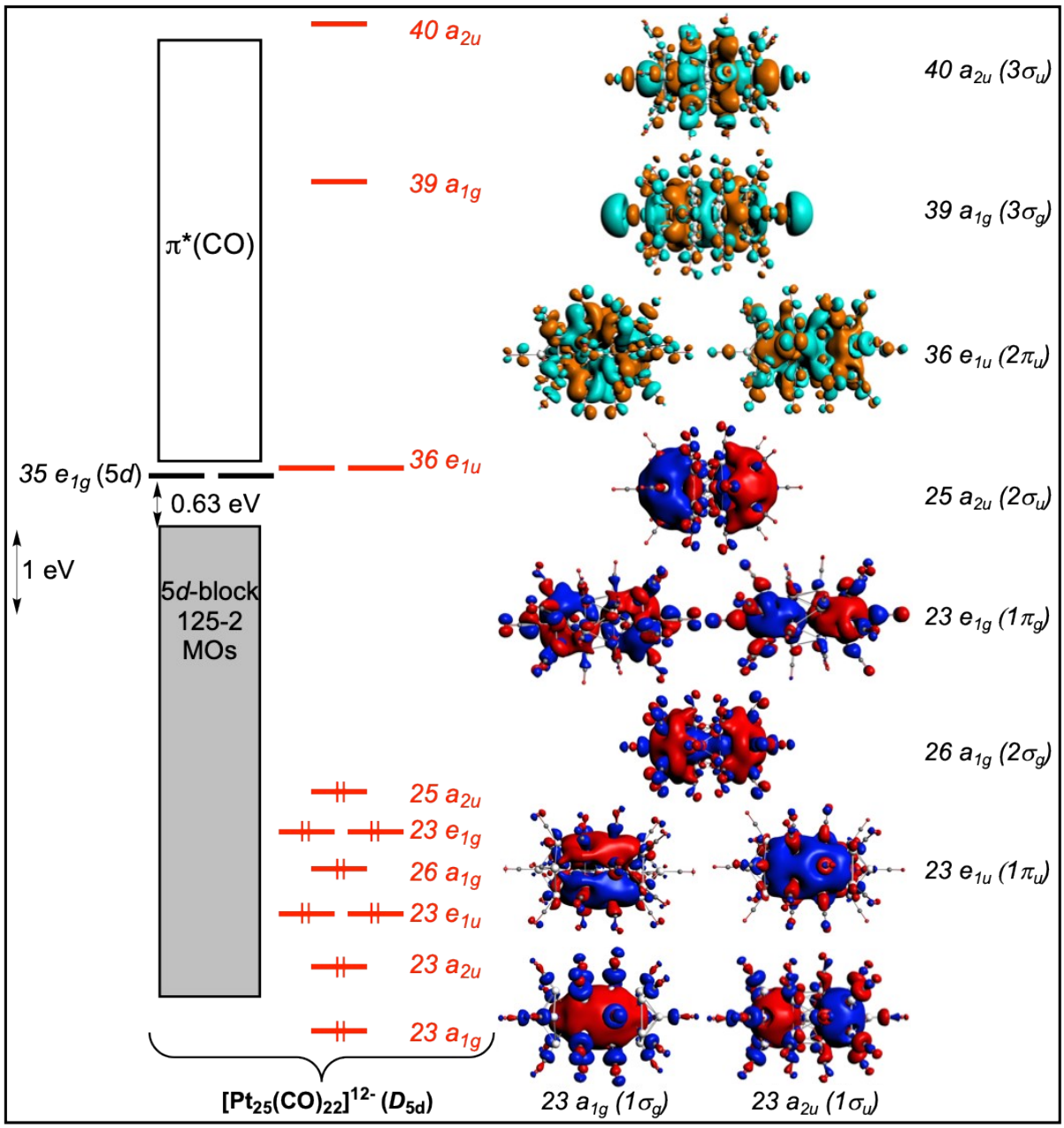

Fig. S14 Kohn-Sham orbital diagram of the hypothetical $Pt_{25}(CO)_{22}]^{12-}$, the core of which is made of three interpenetrating centered icosahedra. The *supermolecular* orbitals plotted on the right side are reminiscent of the valence orbitals of CO_2. The surface isovalue of the inserted plots of *supermolecular* orbitals is ± 0.01 $(e/bohr^3)^{1/2}$.

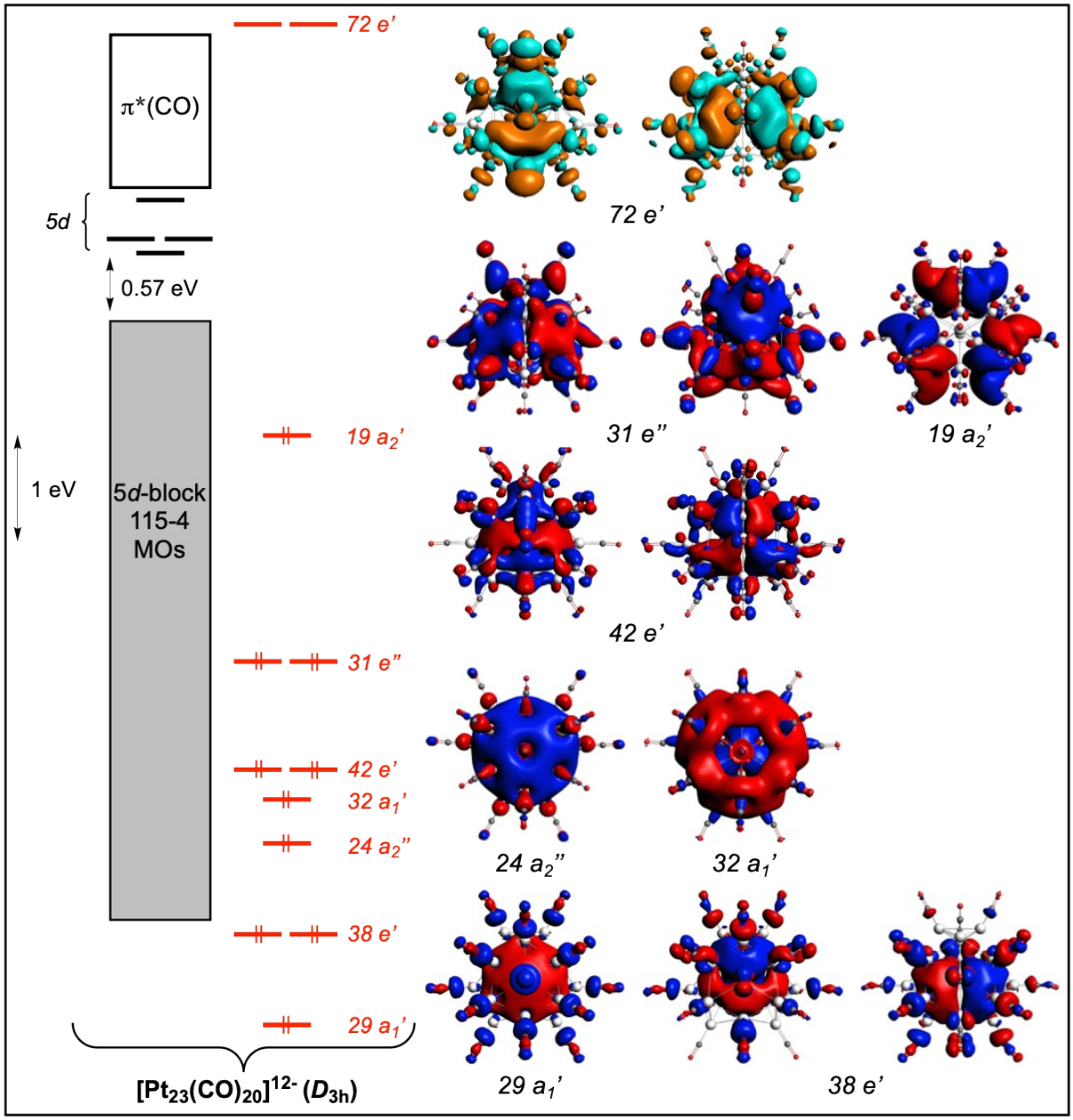

Fig. S15 Kohn-Sham orbital diagram of the hypothetical $[Pt_{23}(CO)_{20}]^{12-}$, the core of which is made of three interpenetrated icosahedra. The *supermolecular* orbitals are plotted on the right side. The surface isovalue of the inserted plots of *supermolecular* orbitals is ± 0.01 $(e/bohr^3)^{1/2}$.

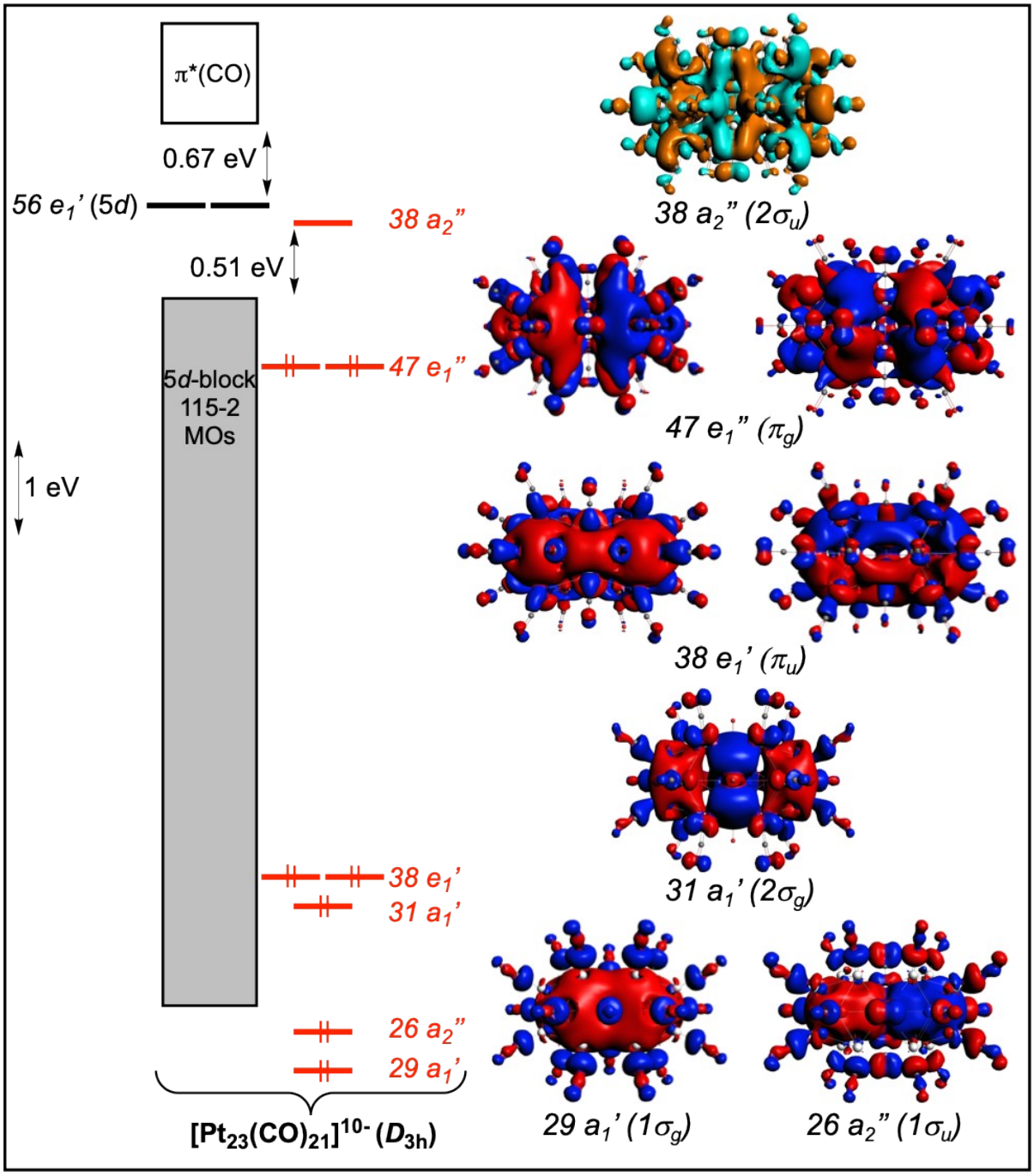

Fig. S16 Kohn-Sham orbital diagram of the hypothetical $[Pt_{23}(CO)_{21}]^{10-}$, the core of which is made of two face-sharing centered icosahedra. The *supermolecular* orbitals, plotted on the right side, are reminiscent of the valence orbitals of F_2. The surface isovalue of the inserted plots of *supermolecular* orbitals is ± 0.01 $(e/bohr^3)^{1/2}$.

Computed model	Metallic kernel structure
$[Pt_{38}(\mu\text{-}CO)_{12}(CO)_{32}]^{2-}$	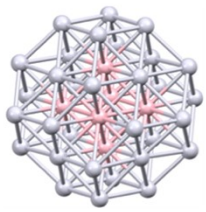
$[Pt_{36}(\mu\text{-}CO)_{18}(CO)_{26}]^{2-}$	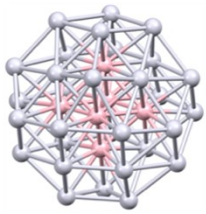
$[Pt_{19}(\mu_3\text{-}CO)_3(\mu\text{-}CO)_3(CO)_{18}(\mu_4\text{-}AuPH_3)_3]^{-}$	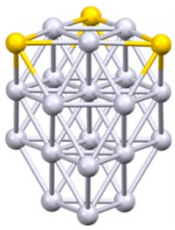
$[Pt_{19}(\mu_3\text{-}CO)(\mu\text{-}CO)_5(CO)_{18}\{\mu_4\text{-}Au_2(PH_3)_2\}_2]$	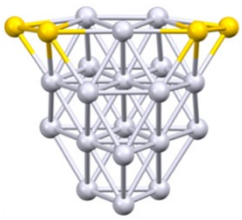
$[Pt_{24}(\mu\text{-}CO)_8(CO)_{22}]^{2-}$	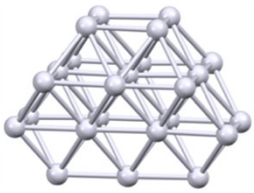
$[Pt_{33}(\mu\text{-}CO)_{10}(CO)_{28}]^{2-}$	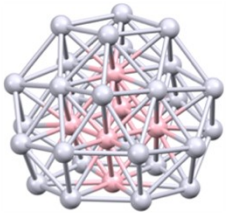
$[Pt_{40}(\mu\text{-}CO)_{16}(CO)_{24}]^{6-}$	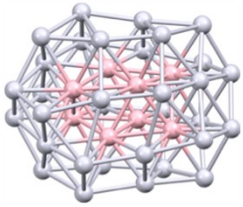

Fig. S17 Metallic kernel structure of various clusters with non-spherical 3D structure. Light-grey, pink and golden-yellow spheres are outer Pt, inner Pt that belong to the encapsulated polyhedron and Au atoms, respectively.

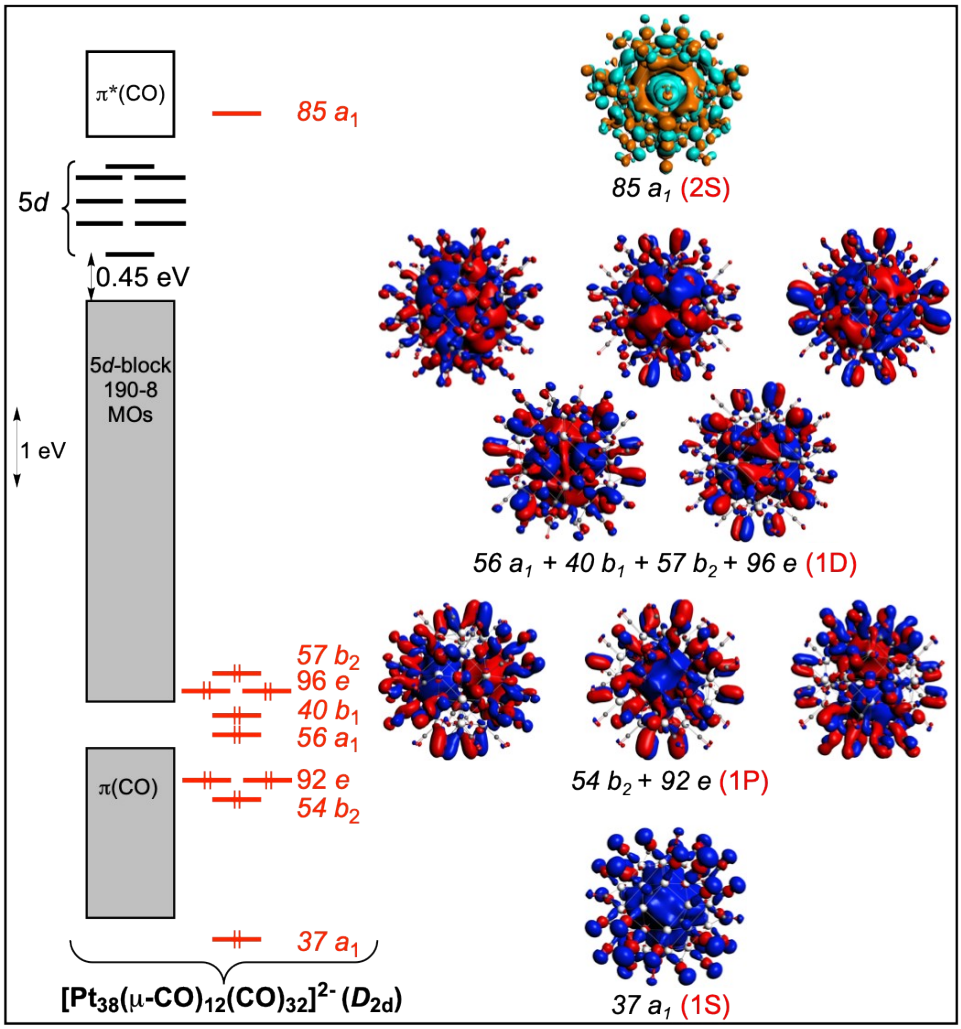

Fig. S18 Kohn-Sham orbital diagram of the pseudo-spherical $[Pt_{38}(\mu_2\text{-}CO)_{12}(CO)_{32}]^{2-}$ ($Pt_6@Pt_{32}$). The *supermolecular* orbitals, plotted on the right side, are consistent with the $1S^2$ $1P^8$ $1D^{10}$ configuration. The surface isovalue of the inserted plots of *superatomic* orbitals is ± 0.01 $(e/bohr^3)^{1/2}$.

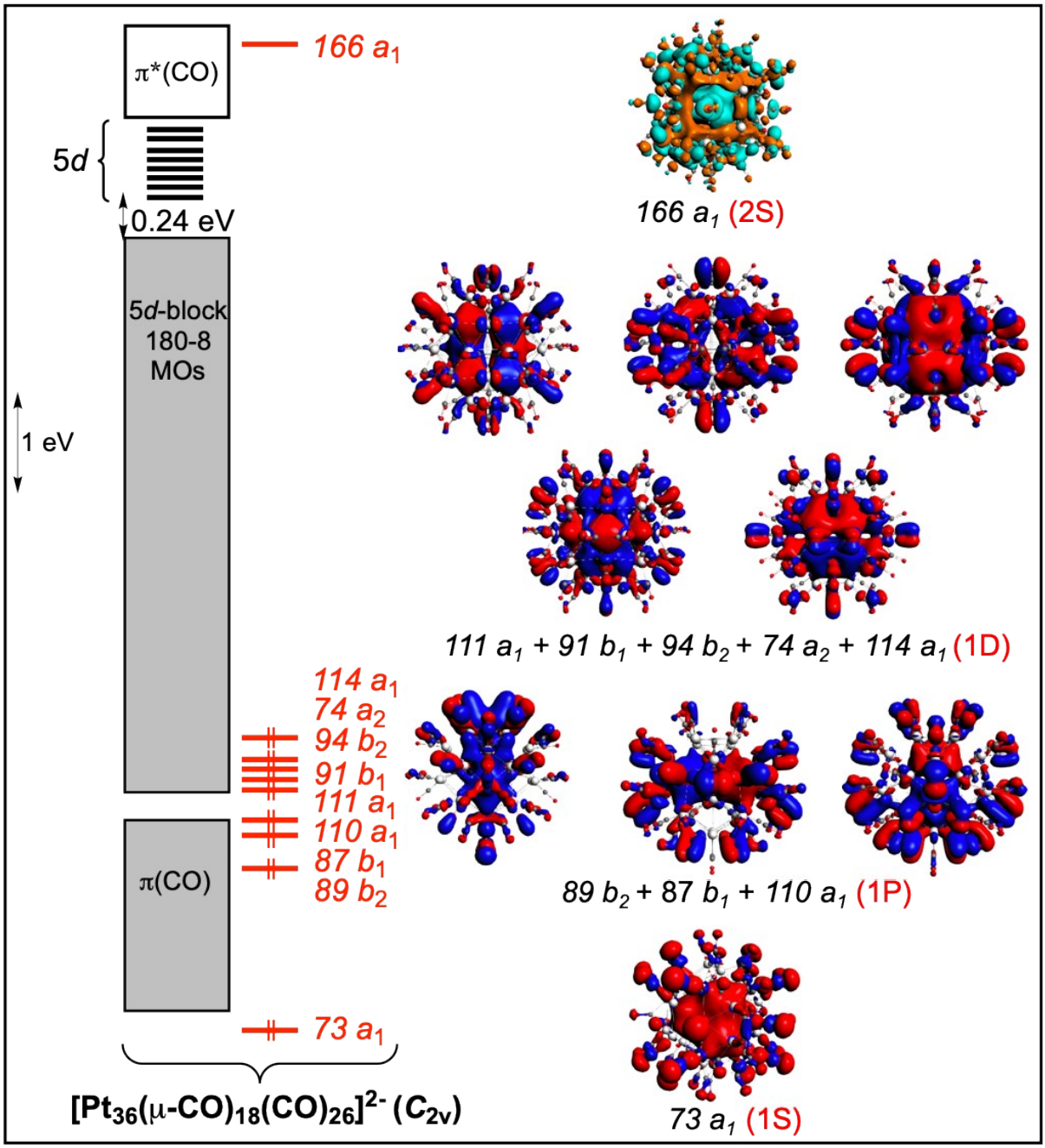

Fig. S19 Kohn-Sham MO diagram of $[Pt_{36}(\mu\text{-}CO)_{18}(CO)_{26}]^{2-}$. The *supermolecular* orbitals, plotted on the right side, are consistent with the $1S^2\ 1P^8\ 1D^{10}$ configuration. The surface isovalue of the inserted plots of *superatomic* orbitals is ± 0.01 $(e/bohr^3)^{1/2}$.

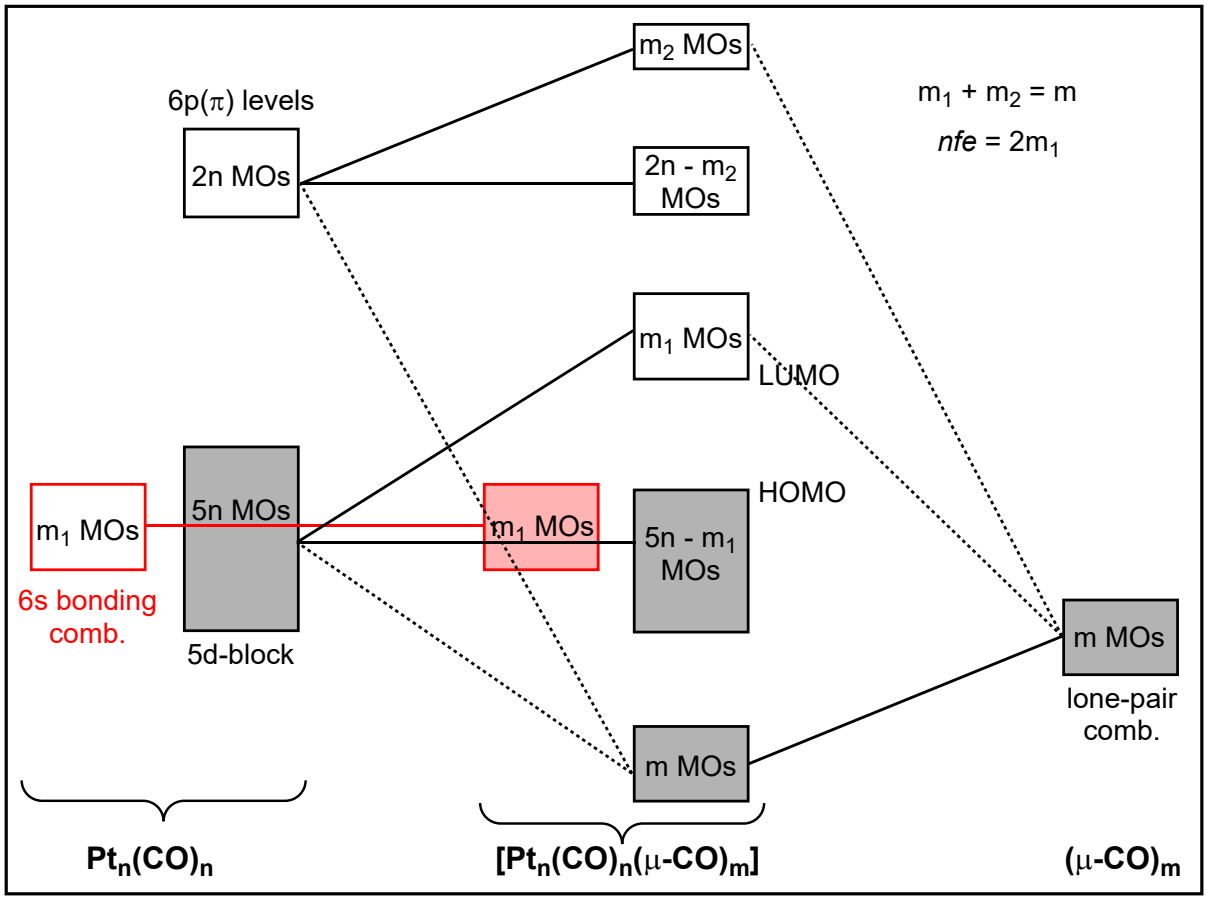

Fig. S20 Simplified MO interaction diagram between the Ptn(CO)n and (μ-CO)m fragments in a neutral [Ptn(CO)n(μ-CO)m] nanocluster with n terminal and m bridging carbonyls (no qualitative change if μ_3-COs in the place of μ-COs). Both the π*(CO) levels and the antibonding 6s(Pt) combinations (all vacant orbitals) are not shown, as well as the n occupied low-lying bonding MOs associated with the n Pt-$CO_{terminal}$ bonds. In the case of a dianionic $[Pt_n(CO)_n(\mu\text{-}CO)_m]^{2-}$ species, for example, then the number of 6s bonding (occupied) combinations would be $m_1 + 1$ and $nfe = 2m_1 + 2$. The bridging COs are necessary to get a closed-shell configuration with the 6s bonding combinations filled but their total number m and the m_1/m_2 ratio are difficult to predict owing to their dependence on complex topological parameters.

Table S1. Relevant computed data for $[Pt_{13}(CO)_{12}]^{8-}$.

		$[Pt_{13}(CO)_{12}]^{8-}$
HOMO-LUMO gap		1.41 eV
Distances (Å) [Wiberg indices]	Pt_c-Pt_p	av. 2.781 [0.1518]
	Pt_p-Pt_p	av. 2.923 [0.0688]
	Pt_p-C	av. 1.829 [1.1925]
NAO Charges (av.)	Pt_c	-0.96
	Pt_p	-0.12
	CO	-0.48

Table S2. Relevant computed data for $[Pt_{13}(CO)_{12}\{Cd_5(\mu\text{-}Br)_5Br_2(dmf)_3\}_2]^{2-}$ The atomic distances are given in Å, Wiberg indices are given in brackets. Experimental bond distances are reported for comparison.

		$[Pt_{13}(CO)_{12}\{Cd_5(\mu\text{-}Br)_5Br_2(dmf)_3\}_2]^{2-}$	
		Calc.	Exp.[1]
HOMO-LUMO gap		1.19 eV	-
$Pt_{cent.}$-$Pt_{vert.}$		2.727-2.757 av. 2.742 [0.1052]	2.696-2.718 av. 2.707
$Pt_{vert.}$-$Pt_{vert.}$		2.765-2.988 av. 2.882 [0.0650]	2.765-2.912 av. 2.850
Cd_{Br}-$Pt_{5\ ring}$		2.868-2.891 av. 2.877 [0.0741]	av. 2.826
Cd_{Br}-Pt_{apical}		3.308-3.321 av. 3.315 [0.0229]	av. 3.262
Cd_{dmf}-$Pt_{5\ ring}$		2.821-2.865 av. 2.843 [0.0954]	av. 2.807
Cd_{dmf}-Pt_{apical}		3.006-3.051 av. 3.022 [0.0536]	av. 3.031
Cd-Br_{br}		2.704-2.822 av. 2.756 [0.2111]	av. 2.711
Cd-$Br_{terminal}$		2.649-2.663 av. 2.656 [0.2975]	av. 2.567
Cd-O		2.388-2.408 av. 2.396 [0.0742]	av. 2.231
Pt-C (Carbonyl)		1.858-1.897 av. 1.873 [0.8318]	av. 1.84
C-O (Carbonyl)		1.156-1.168 av. 1.162 [2.0157]	av. 1.14
NAO charges (av.)	Pt_1	-0.54	-
	Pt_{12}	-0.29	-
	CO	-0.15	-
	L	+1.91	-

Table S3. Relevant computed data for the $Pt_{13}(Au_2L_2)_2(\mu\text{-}CO)_2(CO)_8(L)_4$ (L = CO, PH_3) clusters. Experimental bond distances are reported for comparison.

		$Pt_{13}(Au_2(X)_2)_2(\mu\text{-}CO)_2(CO)_8(X)_4$		
		L = CO	L = PH_3	Exp.[2]
HOMO-LUMO gap		0.96 eV	0.93 eV	
Distances (Å) [Wiberg indices]	Pt_c-Pt_p	av. 2.729 [0.1461]	av. 2.726 [0.1458]	av. 2.707
	Pt_p-Pt_p	av. 2.869 [0.0766]	av. 2.866 [0.0681]	av. 2.846
	Pt_p-Au_b	av. 2.775 [0.1281]	av. 2.779 [0.1316]	av. 2.783
	Au_b-Au_b	av. 3.202 [0.0184]	av. 3.151 [0.0237]	av. 3.131
	Pt_p-CO_t	av. 1.873 [0.8488]	av. 1.864 [0.8887]	av. 1.877
	Pt_p-CO_b	av. 2.048 [0.5759]	av. 2.025 [0.6167]	av. 2.007
	Pt_p-L	av. 1.893 [0.7598]	av. 2.242 [0.4516]	av. 2.260
	Au_b-L	av. 1.928 [0.7622]	av. 2.261 [0.5201]	av. 2.247
NAO Charges (av.)	Pt_c	-0.75	-0.65	
	Pt_p	-0.06	-0.10	
	Au_b	+0.48	+0.31	

Table S4. Relevant computed data for the $Pt_{13}(Pt_2(\mu\text{-}CO)(L)_2)_2(\mu\text{-}CO)_2(CO)_8(L)_4$ (L = CO, PH_3) clusters. Experimental bond distances are reported for comparison.

		$Pt_{13}(Pt_2(\mu\text{-}CO)(L)_2)_2(CO)_{10}(L)_4$		
		L = CO	L = PH_3	Exp.[3]
HOMO-LUMO gap		0.30 eV	0.35 eV	
Distances (Å) [Wiberg indices]	Pt_c-Pt_p	av. 2.728 [0.1452]	av. 2.724 [0.1439]	av. 2.698
	Pt_p-Pt_p	av. 2.869 [0.0804]	av. 2.862 [0.0816]	av. 2.837
	Pt_p-Pt_b	av. 2.768 [0.1316]	av. 2.776 [0.1337]	av. 2.780
	Pt_b-Pt_b	av. 2.936 [0.0964]	av. 2.891 [0.1096]	av. 2.860
	Pt_p-CO_t	av. 1.871 [0.8336]	av. 1.861 [0.8747]	1.64 – 1.83
	Pt_p-CO_b	av. 2.057 [0.5653]	av. 2.030 [0.6086]	1.94 – 2.13
	Pt_p-L	av. 1.896 [0.7534]	av. 2.245 [0.4509]	2.20 – 2.26
	Pt_b-CO_b	av. 2.035 [0.6224]	av. 2.007 [0.6727]	1.94 – 2.13
	Pt_b-L	av. 1.872 [0.9068]	av. 2.219 [0.5774]	2.20 – 2.26
NAO Charges (av.)	Pt_c	-0.76	-0.66	
	Pt_p	-0.02	-0.06	
	Pt_b	+0.28	+0.12	

Table S5. Relevant computed data for the $[Pt_{14}(\mu\text{-}CO)_6(CO)_{12}]^{4-}$ and $[Pt_{15}(\mu\text{-}CO)_8(CO)_{11}]^{4-}$ clusters. Experimental bond distances are reported for comparison.[4,5]

		$[Pt_{14}(\mu\text{-}CO)_6(CO)_{12}]^{4-}$	$[Pt_{15}(\mu\text{-}CO)_8(CO)_{11}]^{4-}$
HOMO-LUMO gap		1.00 eV	1.09 eV
Distances (Å)	Pt_c-Pt_p	av. 2.777 exp. 2.730	av. 2.775 exp. 2.731
	Pt_p-Pt_p	av. 2.867 exp. 2.821	av. 2.874 exp. 2.827
	Pt_p-Pt_b	-	av. 2.753 exp. 2.681
	Pt_p-C_t	av. 1.862 exp. 1.844	av. 1.860 exp. 1.858
	Pt_p-C_b	av. 2.033 exp. 2.004	av. 2.037 exp. 2.011

Table S6. Relevant computed data for the $[Pt_{19}(CO)_{17}]^{8-/10-}$ clusters. Experimental bond distances are reported for comparison.

		$[Pt_{19}(CO)_{17}]^{10-}$	$[Pt_{19}(CO)_{17}]^{8-}$	Exp.[1]
HOMO-LUMO or SOMO-LUMO gap		0.37 eV	Spin-α: 0.47 eV Spin-β: 0.09 eV	
Distances (Å) [Wiberg indices]	Pt_c-$Pt_{c'}$	av. 2.611 [0.0984]	av. 2.571	av. 2.557
	Pt_c-Pt_p	av. 2.813 [0.1298]	av. 2.782	av. 2.730
	Pt_p-Pt_p	av. 2.960 [0.0604]	av. 2.922	av.2.866
	Pt_p-C	av. 1.829 [1.1851]	av. 1.832	av. 1.800
NAO Charges (av.)	Pt_c	-0.80		
	Pt_p	-0.07		
	CO	-0.43		

Table S7. Computed data for $[Pt_{19}(CO)_{17}\{Cd_5(\mu\text{-}Br)_5Br_3(Me_2CO)_2\}\{Cd_5(\mu\text{-}Br)_5Br(Me_2CO)_4\}]^{x-}$ (x = 2, 4). The atomic distances are given in Å. Wiberg indices are given in brackets. Experimental bond distances are given for comparison.

		$[Pt_{19}(CO)_{17}\{Cd_5(\mu\text{-}Br)_5Br_3(Me_2CO)_2\}\{Cd_5(\mu\text{-}Br)_5Br(Me_2CO)_4\}]^{2-}$	$[Pt_{19}(CO)_{17}\{Cd_5(\mu\text{-}Br)_5Br_3(Me_2CO)_2\}\{Cd_5(\mu\text{-}Br)_5Br(Me_2CO)_4\}]^{4-}$	Exp. [1]
HOMO-LUMO or SOMO-LUMO gap (eV)		α-electron: 0.72 eV β-electron: 0.08 eV	0.70 eV	-
Pt_c-Pt_c'		2.594	2.590 [0.1161]	2.557
Pt_c-Pt_p		2.683-2.859 av. 2.761	2.688-2.852 av. 2.770 [0.1184]	2.663-2.793 av. 2.730
Pt_p-Pt_p		2.755-3.043 av. 2.894	2.778-3.112 av. 2.903 [0.0630]	2.775-2.976 av. 2.866
Cd-$Pt_{5\ ring}$		2.789-2.911 av. 2.856	2.774-2.911 av. 2.841 [0.1113]	av. 2.790
Cd-Pt_{apical}		2.939-3.410 av. 3.093	2.911-3.394 av. 3.074 [0.0526]	av. 3.019
Cd-Br_{br}		2.692-2.855 av. 2.765	2.693-3.026 av. 2.812 [0.1775]	av. 2.741
Cd-$Br_{terminal}$		2.621-2.629 av. 2.625	2.650-2.662 av. 2.657 [0.2989]	av. 2.637
Cd-O		2.458-2.488 av. 2.475	2.517-2.555 av. 2.540 [0.0670]	av. 2.350
Pt-C (Carbonyl)		1.848-1.900 av. 1.865	1.841-1.897 av. 1.861 [0.8762]	av. 1.800
C-O (Carbonyl)		1.153-1.169 av. 1.160	1.155-1.174 av. 1.164 [2.0414]	av. 1.170
NAO charges	Pt_{cent}	-	-0.55	
	Pt_{apical}	-	-0.46	
	Pt_{outer}	-	-0.21	
	CO	-	-0.08	
	$Cd_5(\mu\text{-}Br)_5Br_3(Me_2C$	-	+0.62	

	$O)_2$			
	$Cd_5(\mu$ $Br)_5Br(Me_2CO$ $)_4\}$	-	+1.91	

Table S8. Relevant computed data for $[Pt_{19}(\mu\text{-}CO)_{10}(CO)_{12}]^{4-}$. Experimental bond distances are given for comparison.

		$[Pt_{19}(\mu\text{-}CO)_{10}(CO)_{12}]^{4-}$	Exp.[6]
HOMO-LUMO gap		0.80 eV	
Distances (Å) [Wiberg indices]	Pt_c-$Pt_{c'}$	av. 2.710 [0.1309]	av. 2.641
	Pt_c-Pt_p	av. 2.813 [0.1183]	av. 2.794
	Pt_p-Pt_p	av. 2.821 [0.0928]	av. 2.797
	Pt_p-C_t	av. 1.857 [0.9237]	-
	Pt_p-C_b	av. 2.025 [0.5576]	-
NAO Charges (av.)	Pt_c	-0.66	
	Pt_p	+0.13	
	CO	-0.22	

Table S9. Relevant computed data for $[Pt_{26}(\mu\text{-}CO)_9(CO)_{23}]^{2-}$. Experimental bond distances are given for comparison.

	$[Pt_{26}(\mu\text{-}CO)_9(CO)_{23}]^{2-}$	Exp.[4]

HOMO-LUMO gap		0.57 eV	
Distances (Å) [Wiberg indices]	Pt_3-Pt_3	av. 2.813 [0.0630]	av. 2.803
	Pt_3-Pt_p	av. 2.823 [0.1072]	av. 2.801
	Pt_p-Pt_p	av. 2.827 [0.0809]	av. 2.804
	Pt_p-C_t	av. 1.875 [0.8001]	av. 1.840
	Pt_p-C_b	av. 2.029 [0.5536]	av. 1.960
NAO Charges (av.)	Centered Pt_3	-0.63	
	μ_6-Pt_p	-0.07	
	Pt_p	+0.20	
	$Pt_{capping}$	+0.22	
	CO	-0.11	

Table S10. Relevant computed data for $[Pt_{23}(\mu\text{-}CO)_{13}(CO)_{14}]^{2-}$. Experimental bond distances are given for comparison.

		$[Pt_{23}(\mu\text{-}CO)_{13}(CO)_{14}]^{2-}$	Exp.[4]
HOMO-LUMO gap		0.42 eV	
Distances (Å)	Pt_3-Pt_3	av. 2.679	av. 2.655
	Pt_3-Pt_p	av. 2.878	av. 2.808
	Pt_p-Pt_p	av. 2.966	av. 2.936
	Pt_p-C_t	av. 1.874	av. 1.821
	Pt_p-C_b	av. 2.037	av. 2.001

Table S11. Relevant computed data for the hypothetical cluster $[Pt_{25}(CO)_{22}]^{12-}$.

		$[Pt_{25}(CO)_{22}]^{12-}$
HOMO-LUMO gap		0.63 eV
Distances (Å) [Wiberg indices]	Pt_c-$Pt_{c'}$	av. 2.710 [0.0766]
	Pt_c-Pt_p	av. 2.782 [0.1336]
	$Pt_{c'}$-Pt_p	av. 2.831 [0.1178]
	Pt_p-Pt_p	av. 2.988 [0.0596]
	Pt_p-C_t	av. 1.829 [1.1733]
	Pt_p-C_b	-
NAO Charges (av.)	Pt_c	-0.71
	$Pt_{c'}$	-0.79
	Pt_p	-0.04
	CO	=0.40

Table S12. Relevant computed data for the hypothetical cluster $[Pt_{23}CO_{20}]^{12-}$.

		$[Pt_{23}(CO)_{20}]^{12-}$
HOMO-LUMO gap		0.57 eV
Distances (Å)	Pt_3-Pt_3	2.752
	Pt_3-Pt_p	av. 2.822
	Pt_p-Pt_p	av. 3.001
	Pt_p-C	av. 1.831

Table S13. Relevant computed data for the hypothetical cluster $[Pt_{23}CO_{21}]^{10-}$.

		$[Pt_{23}(CO)_{21}]^{10-}$
HOMO-LUMO gap		0.51 eV
Distances (Å)	Pt_c-Pt_p	av. 2.781
	Pt_p-Pt_p	av. 2.951
	Pt_p-C_t	av. 1.843

Table S14. Relevant computed data for $[Pt_{38}(\mu\text{-}CO)_{12}(CO)_{32}]^{2-}$. Experimental bond distances are given for comparison.

		$[Pt_{38}(\mu\text{-}CO)_{12}(CO)_{32}]^{2-}$	Exp.[7]
HOMO-LUMO gap		0.45 eV	
Distances (Å) [Wiberg indices]	Pt_6	av. 2.822 [0.0566]	av. 2.811
	Pt_6-Pt_p	av. 2.838 [0.1141]	av. 2.822
	Pt_p-Pt_p	av. 2.857 [0.0761]	av. 2.845
	Pt_p-C_t	av. 1.880 [0.7805]	av. 1.857
	Pt_p-C_b	av. 2.021 [0.5574]	av. 1.973
NAO Charges (av.)	Centered Pt_6	-0.55	
	Pt_p	+0.17	
	CO	-0.05	

Table S15. Relevant computed data for $[Pt_{36}(\mu\text{-}CO)_{18}(CO)_{26}]^{2-}$. Experimental bond distances are given for comparison.

		$[Pt_{36}(\mu\text{-}CO)_{18}(CO)_{26}]^{2-}$	Exp.[4]
HOMO-LUMO gap		0.24 eV	
Distances (Å)	Pt_6	av. 2.769	av. 2.770
	Pt_6-Pt_p	av. 2.830	av. 2.784
	Pt_p-Pt_p	av. 2.898	av. 2.855
	Pt_p-C_t	av. 1.880	av. 1.833
	Pt_p-C_b	av. 2.050	av. 2.011

Table S16. Relevant computed data for $[Pt_{19}(\mu_3\text{-}CO)_3(\mu\text{-}CO)_3(CO)_{18}(\mu_4\text{-}AuPH_3)_3]^-$. Experimental bond distances are given for comparison.

		$[Pt_{19}(\mu_3\text{-}CO)_3(\mu\text{-}CO)_3(CO)_{18}(\mu_4\text{-}AuPH_3)_3]^-$	Exp.[8]
HOMO-LUMO gap		1.06 eV	
Distances (Å)	Pt_3-Pt_3	av. 2.835	av. 2.816
	Pt_3-Pt_7	av. 2.844	av. 2.782
	Pt_7-Pt_7	av. 2.828	av. 2.796
	Pt_7-Pt_6	av. 2.820	av. 2.796
	Pt_6-Pt_6	av. 2.846	av. 2.833
	Pt_6-$Pt_{3'}$	av. 2.835	av. 2.804
	$Pt_{3'}$-$Pt_{3'}$	av. 2.856	av. 2.859
	Pt-(μ_4-Au)	av. 2.832	av. 2.859
	Pt-C_t	av. 1.882	av. 1.905
	Pt-C_b	av. 2.030	av. 2.072
	Pt-(μ_3-C)	av. 2.158	av. 2.187

Table S17. Relevant computed data for $[Pt_{19}(\mu_3\text{-}CO)(\mu\text{-}CO)_5(CO)_{18}\{\mu_4\text{-}Au_2(PH_3)_2\}_2]$. Experimental bond distances are given for comparison.

		$[Pt_{19}(\mu_3\text{-}CO)(\mu\text{-}CO)_5(CO)_{18}\{\mu_4\text{-}Au_2(PH_3)_2\}_2]$	Exp.[8]
HOMO-LUMO gap		0.94 eV	
Distances (Å)	Pt_3-Pt_3	av. 2.823	av. 2.808
	Pt_3-Pt_7	av. 2.851	av. 2.799
	Pt_7-Pt_7	av. 2.842	av. 2.795
	Pt_7-Pt_6	av. 2.802	av. 2.786
	Pt_6-Pt_6	av. 2.859	av. 2.823
	Pt_6-$Pt_{3'}$	av. 2.840	av. 2.799
	$Pt_{3'}$-$Pt_{3'}$	av. 2.835	av. 2.823
	Pt-(μ_4-Au)	av. 2.828	av. 2.838
	Pt-C_t	av. 1.886	av. 1.885
	Pt-C_b	av. 2.037	av. 1.983
	Pt-(μ_3-C)	av. 2.150	av. 2.146

Table S18. Relevant computed data for $[Pt_{40}(\mu\text{-}CO)_{16}(CO)_{24}]^{6-}$. Experimental bond distances are given for comparison.

		$[Pt_{40}(\mu\text{-}CO)_{16}(CO)_{24}]^{6-}$	Exp.[9]
HOMO-LUMO gap		0.25 eV	
Distances (Å)	Pt_8	av. 2.762	av. 2.745
	Pt_8-Pt_p	av. 2.773	av. 2.737
	Pt_p-Pt_p	av. 2.874	av. 2.883
	Pt_p-C_t	av. 1.860	av. 1.851
	Pt_p-C_b	av. 2.023	av. 1.978

Table S19. Relevant computed data for $[Pt_{24}(\mu\text{-}CO)_8(CO)_{22}]^{2-}$. Experimental bond distances are given for comparison.

		$[Pt_{24}(\mu\text{-}CO)_8(CO)_{22}]^{2-}$	Exp.[4]
HOMO-LUMO gap		0.66 eV	
Distances (Å)	Pt_{10}-Pt_{10}	av. 2.826	av. 2.803
	Pt_{10}-Pt_9	av. 2.850	av. 2.826
	Pt_9-Pt_9	av. 2.819	av. 2.797
	Pt_9-Pt_5	av. 2.843	av. 2.819
	Pt_5-Pt_5	av. 2.824	av. 2.796
	Pt-C_t	av. 1.878	av. 1.860
	Pt-C_b	av. 2.033	av. 1.996

Table S20. Relevant computed data for $[Pt_{33}(\mu\text{-}CO)_{10}(CO)_{28}]^{2-}$. Experimental bond distances are given for comparison.

		$[Pt_{33}(\mu\text{-}CO)_{10}(CO)_{28}]^{2-}$	Exp.[4]
HOMO-LUMO gap		0.49 eV	
Distances (Å)	Pt_8-Pt_8	av. 2.858	av. 2.828
	Pt_8-Pt_{12}	av. 2.838	av. 2.815
	Pt_{12}-Pt_{12}	av. 2.824	av. 2.827
	Pt_{12}-Pt_9	av. 2.850	av. 2.818
	Pt_9-Pt_9	av. 2.823	av. 2.796
	Pt_9-Pt_4	av. 2.856	av. 2.829
	Pt_4-Pt_4	av. 2.882	av. 2.837
	Pt-C_t	av. 1.876	av. 1.857
	Pt-C_b	av. 2.028	av. 1.996

References

1. C. Femoni, M. C. Iapalucci, G. Longoni, S. Zacchini and S. Zarra, *J. Am. Chem. Soc*., 2011, **133**, 2406–2409.
2. N. de Silva and L.F. Dahl, *Inorg. Chem*., 2005, **44**, 9604–9606.
3. L. V. Nair, S. Hossain, S. Wakayama, S. Takagi, M. Yoshioka, J. Maekawa, A. Harasawa, B. Kumar, Y. Niihori, W. Kurashige and Y. Negishi, *J. Phys. Chem. C,* 2017, **121**, 11002–11009.
4. E. Cattabriga, I. Ciabatti, C. Femoni, M. C. Iapalucci, G. Longoni and S. Zacchini, *Inorg. Chim. Acta,* 2018, **470**, 238–249.
5. F. Gao, C. Li, B. T. Heaton, S. Zacchini, S. Zarra, G. Longoni and M. Garland, *Dalton Trans.,* 2011, **40**, 5002–5008.
6. D. M. Washecheck, E. J. Wucherer, L. F. Dahl, A. Ceriotti, G. Longoni, M. Manassero, M. Sansoni and P. Chini, *J. Am. Chem. Soc*., 1979, **101**, 6110–6112.
7. A. Ceriotti, N. Masciocchi, P. Macchi and G. Longoni, *Angew. Chem. Int. Ed*., 1999, **38**, 3724–3727.
8. A. Ceriotti, P. Macchi, A. Sironi, S. El Afefey, M. Daghetta, S. Fedi, F. Fabrizi de Biani and R. Della Pergola, *Inorg. Chem*., 2013, **52**, 1960–1964.

9. E. Cattabriga, I. Ciabatti, C. Femoni, T. Funaioli, M. C. Iapalucci and S. Zacchini, *Inorg. Chem*., 2016, **55**, 6068–6079.